Biochemical Pharmacology 79 (2010) 1781–1790

Contents lists available at ScienceDirect

Biochemical Pharmacology

journal homepage: www.elsevier.com/locate/biochempharm

Remarkable interference with telomeric function by a G-quadruplex selective bisantrene regioisomer

Marco Folini [a], Claudia Pivetta [b], Giuseppe Zagotto [b], Cinzia De Marco [a], Manlio Palumbo [b], Nadia Zaffaroni [a], Claudia Sissi [b,*]

[a] Department of Experimental Oncology and Molecular Medicine, Fondazione IRCCS Istituto Nazionale dei Tumori, Via Venezian 1, 20133 Milano, Italy
[b] Department of Pharmaceutical Sciences, University of Padua, Via Marzolo 5, 35131 Padova, Italy

ARTICLE INFO

Article history:
Received 8 January 2010
Accepted 24 February 2010

Keywords:
Alternative lengthening of telomeres
Bisantrene
G-quadruplex
Telomerase
Telomere

ABSTRACT

The use of small molecules able to induce and stabilize selected G-quadruplex arrangements can cause telomerase inhibition and telomere dysfunction in cancer cells, thus providing very selective therapeutic approaches. Effective stabilizers usually comprise a planar aromatic portion to grant effective stacking onto the G-quartet and positively charged side chains to exploit the highly negative charge density on the quadruplex grooves. Since the relative position of these two pharmacophoric moieties is expected to play an important role in DNA folding stabilization, we evaluated a series of anthracene derivatives substituted with one or two 4,5-dihydro-1*H*-imidazol-2-yl-hydrazonic groups (the bisantrene side chain) at different positions of the aromatic system. Indeed, the various regioisomers showed distinct binding affinities for telomeric G-quadruplex, and the most effective was the 1,5 and 1,7 bis-substituted analogues. On turn, the 1,8 regioisomer was poorly effective. Interestingly, G-quadruplex binding is clearly related to telomerase inhibition in this class of compounds, thus confirming their ability to shift the nucleic acid conformational equilibrium upon binding and consequently produce interference with the telomere processing enzyme. Additionally, the 1,5 regioisomer was shown to inhibit telomerase activity at lower concentrations than those required to reduce tumor cell proliferation. Comparative analysis of drug effects in telomerase-positive and telomerase-negative cancer cells showed consistent cell growth impairment, as a consequence of activation of the senescence pathway, which was mainly attributable to anthracene-mediated telomere dysfunction.

1. Introduction

Telomerase is a ribonucleoprotein reverse transcriptase responsible for telomere length maintenance [1]. Its expression is associated with cell immortalization and tumorigenesis since it is expressed in most human tumor cells but is not active in most somatic cells [2]. In the last decade, several classes of telomerase machinery inhibitors have been evaluated as potential anticancer agents. Study of their pharmacological properties revealed different pathways related to interference with telomerase activity [3]. Generally, inhibition of telomerase results in cellular senescence or apoptosis in a time-dependent manner that correlates with the initial telomere length [4]. Alternatively, tumor cell crisis can be rapidly induced by promoting telomere dysfunction. Indeed, many proteins are involved in preserving a complex telomere architecture [5]: when it collapses a signaling cascade comparable to that promoted by DNA damage is activated and cell cycle arrest (accelerated senescence) or apoptosis is induced [6].

Telomerase substrates are the telomeres, double-stranded DNA portions with a 3′ protruding overhang (100–200 bases long), formed by a repeating noncoding sequence (TTAGGG in humans) [7,8]. In analogy to other G-rich sequences, the single-stranded portion can fold into a structure called G-quadruplex [9]. These folding results of overlapping planar regions were identified by four Hoogsten-paired guanines [10]. By recognizing and stabilizing this peculiar DNA arrangement, selected ligands impair telomere–telomerase interaction thus interfering with the telomere elongation step catalyzed by the enzyme [11]. Additionally, they can displace the telomere binding proteins (i.e., TRF2 and hPOT1) involved in telomere capping, thereby allowing recognition of the free terminal sequence as a DNA damage region [12]. To date, several compounds able to interact with and stabilize G-quadruplex structures formed by G-rich single-stranded overhangs of telomeres have been identified. They include anthraquinones

* Corresponding author. Tel.: +39 49 8275711; fax: +39 49 8275711.
E-mail addresses: marco.folini@istitutotumori.mi.it (M. Folini), claudia.pivetta@unipd.it (C. Pivetta), giuseppe.zagotto@unipd.it (G. Zagotto), cinzia.demarco@istitutotumori.mi.it (C. De Marco), manlio.palumbo@unipd.it (M. Palumbo), nadia.zaffaroni@istitutotumori.mi.it (N. Zaffaroni), claudia.sissi@unipd.it (C. Sissi).

0006-2952/$ – see front matter © 2010 Elsevier Inc. All rights reserved.
doi:10.1016/j.bcp.2010.02.018

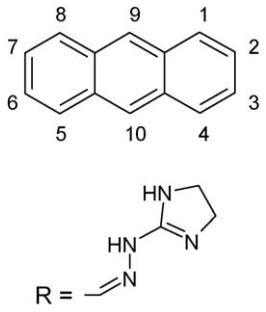

derivative	R at position
Ant1	1
Ant1,5	1 & 5
Ant1,8	1 & 8
Ant2	2
Ant2,6	2 & 6
Ant2,7	2 & 7
Ant9	9
Ant9,10 (Bisantrene)	9 & 10

Fig. 1. Chemical structure of tested compounds.

[13–15], fluorenones [16], acridines [17,18], triazine [19], cationic porphyrins [20], and perylenes [21], just to name a few. They share a general consensus structural motif based on a large flat aromatic surface linked to protonable side chains. DNA binding occurs mainly through stacking on a terminal G-tetrad, whereas side chains contribute to the stability of the complex by hydrophobic/ionic interactions into the DNA grooves [7].

Since similar basic features characterize intercalation and base stacking, the scaffolds of classical intercalating agents are commonly used as the starting structures to produce G-quadruplex recognition. Literature data have proven that, by working on the number, the length and the position of the charged side chains bound to a "classical" intercalator, it is possible to preferentially direct drug binding towards G-quadruplex forms. Indeed, such an approach led to the identification of effective G-quadruplex binders such as the tri-substituted acridine BRACO 19 and the 2,6 or 2,7 bis-substituted amido-anthraquinones. These binders are characterized by poor cytotoxicity and are able to induce a reduction in telomere length upon long-term drug exposure [17,22–24].

Bisantrene is a known intercalating agent and an excellent topoisomerase-II poison [25]. In a previous work, we demonstrated that the number and location of bisantrene side chains modulate cytotoxicity and topoisomerase-II-associated DNA cleavage [26–28]. Additionally, a lower enzyme poisoning efficiency was not always associated with decreased cytotoxicity, suggesting that alternative pharmacologically relevant mechanism(s) were operating.

Bisantrene shares the structural "consensus motif" characteristic of effective G-quadruplex binders, thus possible relationships between telomerase/telomere interference and biological effects can be envisaged. To address the issue, in the present study we prepared and examined a series of anthracene derivatives substituted with one or two 4,5-dihydro-1*H*-imidazol-2-yl-hydrazonic groups (the bisantrene side chain) at different positions of the aromatic system (Fig. 1). All derivatives were tested for interaction with DNA in different conformations and the relationships between DNA recognition and telomerase inhibition at a molecular and cellular level was examined. This allows us to suggest possible relationships between type and stability of the drug-nucleic acid complex formed and the resulting cellular cytoxicity pathways. Finally, telomerase-independent cell growth inhibitory activity of the best bisantrene regioisomer was evaluated on telomerase-negative tumor cells, which maintain their telomeres through an alternative lengthening of telomeres (ALT) mechanism [29], a recombination-based telomere elongating mechanism preferentially expressed in human tumors of mesenchymal origin [30].

2. Materials and methods

2.1. Drugs and reagents

All drugs were synthesized according to a previously reported protocol [26]. Their structure and purity were confirmed by high performance liquid chromatography, nuclear magnetic resonance and mass spectrometry techniques. Stock solutions were prepared in DMSO and freshly diluted in the required buffer.

The human telomeric sequence HTS 5′ Dabcyl-AGGGTTAGGGT-TAGGGTTAGGGT-FAM 3′ was synthesized and purified by Atdbio (Southampton, UK). Its complementary strand 4GGGdown, ACCCTAACCCTAACCCTAACCCT; Tel22, AGGGTTAGGGTTAGGGT-TAGGG; 2GGG, TACAGATAGTTAGGGTTAGGGTTA; 1GGG, TACAGA-TAGTTAGGGTTAGACTTA; QMup, 5′ FAM- GTGAGATACCGACAG-AAG; QMdown, CTTCTGTCGGTATCTCAC- Dabcyl 3′; Tup, 5′-TGAGGATCCGCCTGGACAGCATGG-3′ and Tdown, 5′-GTCGAATTC-TCGGCGAGAAGCAGG-3′ were synthesized by Eurogentec (Seraing, Belgium). Calf thymus DNA (ctDNA) was purchased from Sigma Aldrich (St.Louis, MO, USA).

2.2. Taq polymerase assay

Compounds were assayed against *Taq* polymerase by using pBR322 (2.5 ng) as a DNA template and appropriate primer sequences Tup and Tdown (0.5 μM) to amplify the 906–1064 sequence of plasmid by polymerase chain reaction (PCR). The reaction was carried out in a PerkinElmer thermocycler (Waltham, MA, USA), performing 25 cycles (30 s at 94 °C, 30 s at 58 °C and 30 s at 72 °C). The reaction products were resolved on a 2% agarose gel in TBE buffer (89 mM Tris base, 89 mM boric acid, 2 mM Na_2EDTA) and stained by ethidium bromide.

2.3. Evaluation of telomerase activity

Telomerase activity was measured on 1 μg of protein by the telomeric-repeat amplification protocol (TRAP) using the TRAPeze kit (Millipore S.p.A., Vimodrone, Italy), according to the manufacturer's protocol. Each reaction product was amplified in the presence of a 36-bp internal TRAP assay standard. A TSR8 quantification standard (which serves as a standard to estimate the amount of product extended by telomerase in a given protein extract) was included for each set of TRAP assays. PCR amplification products were then resolved by polyacrylamide gel electrophoresis and visualized by Sybr Green I (Sigma–Aldrich; St.Louis, MO, USA) staining (cell-free experiments, unlabelled telomeric substrate) or autoradiography (cell-based experiments, ^{32}P-end-labeled telomeric substrate). Quantitative analysis was performed with Image-QuanT software (Molecular Dynamics, Sunnyvale, CA, USA), which allowed densitometric evaluation of the digital image. Telomerase activity was quantified by measuring the signal of telomerase ladder bands, and the relative telomerase activity was calculated as the ratio to the internal standard using the following formula:

$$\text{relative telomerase activity} = \left[\frac{(X - X_0)}{C}\right] \times \left[\frac{(R - R_0)}{\text{Cr}}\right]^{-1}$$

where X is the untreated sample, X_0 is the RNase-treated sample, C is the internal control of untreated samples, Cr is the internal control of TSR8, R is the TSR8 quantification control, and R_0 is the negative control.

2.4. DNA binding studies

Fluorometric measurements were performed with a PerkinElmer LS30 fluorometer equipped with a Haake F3-C thermostat. Titrations were carried out at 25 °C in 10 mM Tris–HCl, pH 7.0, 1 mM EDTA and KCl to obtain the desired ionic strength. Binding was followed by addition of increasing amounts of DNA to a freshly prepared drug solution. To avoid large systematic inaccuracies due to experimental errors, the range of bound drug fractions utilized for calculations was 0.15–0.85. For Tel22, the

experimental data were analyzed according to equation 1, which describes a 1:1 binding mode:

$$\frac{\Delta F}{\Delta F_{\max}} = \frac{\{[L_0] + [G_0] + K_d - [([L_0] + [G_0] + K_d)^2 - 4 \times [L_0] \times [G_0]]^{1/2}\}}{(2 \times [L_0])} \quad (1)$$

where L_0 and G_0 are the ligand and G-quadruplex concentration, respectively.

For calf thymus DNA, data were evaluated according to the equation of McGhee and Von Hippel [31] for non-cooperative ligand–lattice interactions:

$$\frac{r}{m} = \frac{K_i(1 - nr)^n}{[1 - (n-1)r]^{n-1}} \quad (2)$$

where r is the molar ratio of bound ligand to DNA, m is the free ligand concentration, K_i the intrinsic binding constant, and n the exclusion parameter.

2.5. Fluorescence melting studies

The melting temperature of fluorescein-labeled DNA in the presence or absence of ligands was determined by fluorescence melting experiments performed in a Roche LightCycler, using an excitation source at 488 nm. The changes in fluorescence emission were recorded at 520 nm.

Melting experiments were performed in a total volume of 20 μl containing 0.25 μM quadruplex-forming oligonucleotide and variable concentrations of tested derivatives in LiP buffer (10 mM LiOH; 50 mM KCl, pH 7.4, with H_3PO_4). When G-quadruplex versus duplex selectivity studies were performed, stoichiometric amounts of complementary strand were added. For duplex stabilization experiments, QMup and QMdown were mixed at equimolar concentrations, heated to 95 °C for 5 min, and cooled to room temperature overnight. Mixtures were first denatured by heating to 95 °C at a rate of 0.5 °C/min and keeping this temperature for 5 min. They were then cooled to 30 °C at the rate of 0.5 °C/min. Recordings were taken during both the melting and annealing reactions to check for hysteresis. T_m values were determined from the first derivatives of the melting profiles using the Roche LightCycler software.

2.6. Electrophoretic mobility shift assay

Single-stranded DNA (2GGG or 1 GGG) was 5′-labeled with ^{32}P using T4 polynucleotide kinase. A mixture of purified labeled and unlabelled oligonucleotides (total final concentration, 10 μM) was heated to 95 °C for 5 min in 10 mM Tris–HCl, 1 mM EDTA, 100 mM KCl, pH 8.0, buffer and cooled overnight at room temperature. After the DNA folding step, 5 μl of test compound was dispensed to each sample to produce the required ligand concentrations in a total volume of 20 μl. Reaction mixtures were incubated at 37 °C for 24 h and subsequently analyzed by native 16% polyacrylamide gel in TBE 0.5× containing 20 mM KCl running buffer. Resolved bands on dried gels were visualized and quantified on a PhosphorImager.

2.7. Cell-based experiments

Human melanoma (SK-Mel5), colon cancer (LoVo) and osteogenic sarcoma (U2OS) cell lines were obtained from American Type Culture Collection (Rockville, MD, USA). Cells were maintained as a monolayer in the logarithmic growth phase at 37 °C in a 5% CO_2 humidified atmosphere, using Dulbecco's modified Eagle's medium (SK-Mel5 and LoVo) and McCoy's 5A medium (U2OS) provided by Lonza (Verviers, Belgium) and supplemented with 10% fetal calf serum and 0.1% gentamycin.

In the short-term cell growth assay, cells were seeded at the appropriate density in 25 cm^2 tissue culture flasks and exposed to increasing concentrations (2.5, 5, 10, 20 μM) of freshly dissolved compounds. Adherent and floating cells were collected, counted in a particle counter (Coulter Counter, Coulter Electronics, Luton, UK) after 24, 48 and 96 h of drug exposure, and the IC_{50} (drug concentration inhibiting cell growth by 50%) value for each drug was calculated. In the long-term cell growth assay, SK-Mel5 and U2OS cells were seeded at appropriate density in 25 cm^2 tissue culture flasks, exposed to 2.5 μM Ant1,5 for 48 h, washed and then cultured for an additional 144 h. In the case of SK-Mel 5, the culture medium was removed every 48 h, and fresh medium containing the same drug concentration was added to the cultures. Floating and adherent cells were collected and counted as described above every 48 h.

Cell cycle analysis was performed by a fluorescent-activated cell sorter (FACScan, Becton Dickinson, Franklin Lake, NJ, USA) on untreated or treated cells fixed in pre-cooled 70% ethanol and stained with a solution containing 50 μg/ml propidium iodide, 50 mg/ml RNase and 0.05% Nonidet P40 for 30 min at 4 °C. A minimum of 3×10^4 events was measured for each sample, and the cell distribution in the different phases of the cell cycle was detected on DNA plots by CellQuest software according to the Modfit model (Becton Dickinson, Franklin Lakes, NJ, USA). An aliquot of propidium iodide-stained cells was spotted onto glass slides and examined under a fluorescence microscope for the presence of nuclei with apoptotic morphology. The percentage of apoptotic cells was determined by scoring at least 300 cells for each sample.

To evaluate the induction of senescence, untreated and Ant1, 5-treated cells were stained using the senescence β-galactosidase staining kit (Cell Signaling Technology, Danvers, MA). Briefly, cells were fixed in 2% formaldehyde/0.2% glutaraldehyde for 15 min at room temperature, rinsed twice with phosphate buffered saline, stained with 1 ml of a Staining Solution mix prepared according to manufacturer's instruction and containing 1 mg/ml X-gal (5-bromo-4-chloro-3-indolyl-β-D-galactopyranoside). After an overnight incubation at 37 °C cells were checked under a microscope for development of blue color.

2.8. Immunoblotting and immunofluorescence analyses

For immunoblotting, 40 μg of protein extracts was fractioned by SDS-PAGE and transferred onto Hybond nitrocellulose membranes (GE Healthcare, UK). Filters were blocked in PBS-Tween-20 in 5% skim milk and probed with antibodies raised against $p21^{waf1}$ and trimethyl K9 Histone H3 (Abcam, Cambridge, UK), that were subsequently visualized by SuperSignal® West PICO chemiluminescent detection system (Thermo Scientific, Rockford, IL, USA) after being probed with secondary anti-mouse horseradish peroxidase-linked whole antibody (GE Healthcare, UK). B-actin was used as an equal protein loading control.

For immunofluorescence analysis, SK-Mel5 and U2OS cells grown on glass coverslips were fixed with 4% formaldehyde and probed with primary anti-γ-H2AX (Abcam, Cambridge, MA, USA) and secondary AlexaFluor594 (Invitrogen, Carlsbad, CA, USA) antibodies. For the co-localization of γ-H2AX foci at the telomere, fixed cells were processed by combined γH2AX indirect immunofluorescence and telomere fluorescence *in situ* hybridization by using the 5'labeled Cy3-(5′-CCCTAA-3′)$_3$ PNA probe (Applied Biosystems, Framingham, MA, USA). Images were acquired by a Nikon Eclipse E600 microscope using ACT-1 software (Nikon Corporation, Japan) and processed with an Adobe Photoshop Image Reader 7.0.

3. Results

3.1. Number and position of side chains affect anthracene-G-quadruplex interaction

The ability of tested compounds to induce G-quadruplex folding of a human telomeric sequence was evaluated by electromobility shift assays. In these experiments, we used oligos 1GGG and 2GGG in the presence of 100 mM KCl. These sequences can form intermolecular G-quadruplex structures (dimeric or tetrameric) that migrate slower than non-structured single-stranded DNA (Fig. 2a).

None of the tested compounds was able to induce the folding of tetrameric G-quadruplex structures formed by the 1GGG sequence. Regarding the 2GGG sequence, only di-substituted bisantrene analogues were able to induce dimeric G-quadruplex structures, albeit to different extents. In particular, the most efficient derivatives were Ant1,5 followed by Ant2,6 and Ant2,7, as shown by the quantitative determination of G-quadruplex induction summarized in Fig. 2b.

To further investigate the ability of tested compounds to stabilize G-quadruplex structures, we performed fluorescence melting experiments. We used a four human telomeric repeats sequence which forms an intramolecular mixed-type G-quadruplex structure [32], labeled with a fluorophore and a quencher at the 3′ and 5′ end, respectively. Using this substrate, we compared the melting temperature of the G-quadruplex arrangement in the presence and absence of increasing concentrations of tested compounds. All anthracene derivatives were able to increase the thermal stability of the folded oligonucleotide, hence producing a stabilizing effect on the G-quadruplex structure, although to a widely varying extent.

Fig. 3a shows the ΔT_m (increase in melting temperature) values obtained at a constant ligand concentration (2.5 μM). As expected, mono-substituted derivatives showed almost negligible G-quadruplex stabilization. Among di-substituted anthracenes, the efficiency order for T_m increment perfectly matched that reported for G-quadruplex induction, with Ant1,5 producing the largest stabilization, followed by 2,6- and 2,7-substituted derivatives. In turn, Ant9,10 and Ant1,8 exhibited a poor efficiency in G-quadruplex stabilization.

3.2. Anthracene derivatives selectively stabilized G-quadruplex folding

A drawback of G-quadruplex binders containing a planar surface is represented by their possible concomitant recognition of double-stranded DNA. To assess this point for anthracene derivatives, melting experiments were performed using a non-G-quadruplex-forming sequence paired to its complementary strand to form a double helix (oligos QMup and QMdown). Data are summarized in Fig. 3b. As expected, mono-substituted derivatives poorly stabilized both DNA arrangements, whereas Ant9,10 was able to induce a good stability of the duplex arrangement followed by Ant1,5 and Ant1,8. From these data, Ant9,10 and Ant1,8 do not appear to discriminate efficiently between the two tested DNA

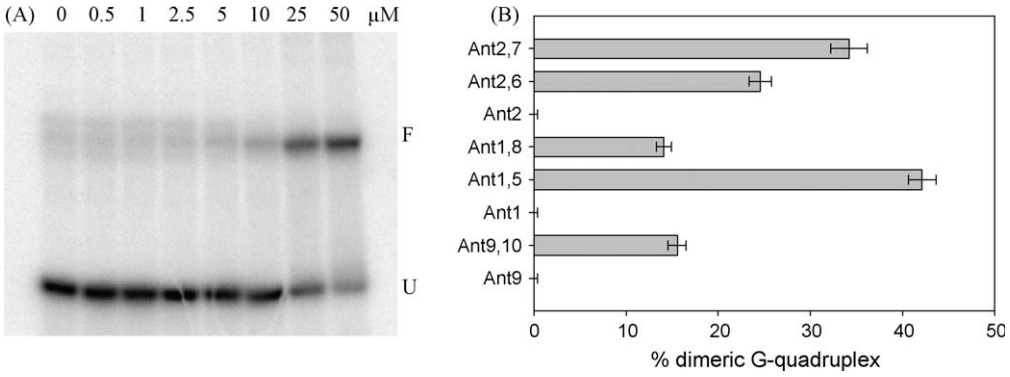

Fig. 2. Induction of G-quadruplex structures by tested derivatives. (a) Effect of increasing Ant1,5 concentrations on the assembly of 2GGG (10 μM strand concentration) into dimeric G-quadruplex structure in 10 mM Tris, 1 mM EDTA, 100 mM KCl at pH 8.0, after incubation at 37 °C for 24 h. Reaction products were resolved on a 16% native polyacrylamide gel in TBE 0.5× containing 20 mM KCl. U and F refer to the unfolded and G-quadruplex folded DNA respectively. (b) Percentage of dimeric G-quadruplex structure, formed by oligonucleotide 2GGG, induced by tested derivatives. Reported values refer to a 25 μM concentration of compounds.

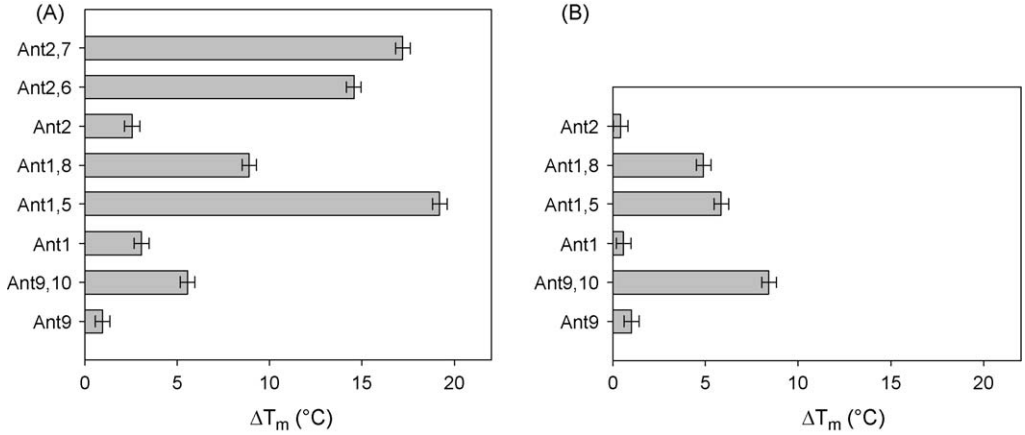

Fig. 3. Variation of thermal stability of different DNA folding induced by tested derivatives. ΔT_m values obtained by melting experiments on G-quadruplex structured 4GGG (2.5 μM) (a) or double-stranded DNA (2.5 μM) (b). All data refer to a 5 μM final concentration of ligand.

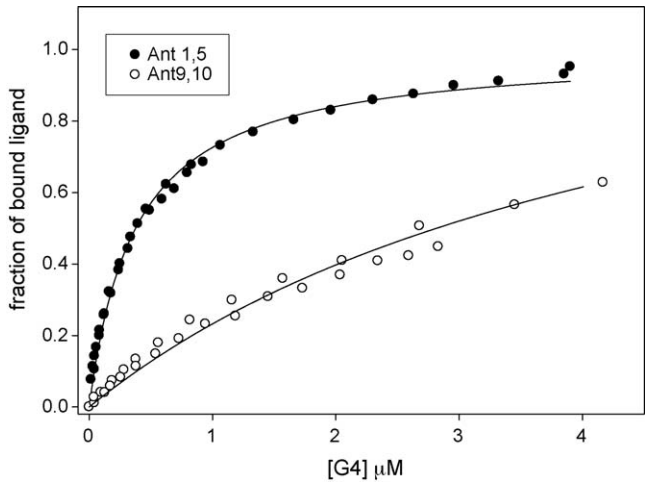

Fig. 4. Binding isotherm for Ant9,10 (○) and Ant 1,5 (●) to G-quadruplex folded Tel22 determined in 10 mM Tris, pH 8.0, 1 mM EDTA, KCl up to 0.5 M ionic strength. Solid lines correspond to the best fit based on Eq. (1).

conformations (comparable ΔT_m), thus supporting the absence of a selective recognition. On the contrary, Ant1,5 exhibited a substantially larger preference for G-quadruplex structures. Melting studies on 4GGG recorded in the presence of stoichiometric amounts of its complementary sequence allowed to simultaneously evaluate the thermal stabilization of double-stranded and of G-quadruplex arrangements. The experimental findings totally agree with the previous results (see Supplementary Material, Fig S1).

It is noteworthy that Ant2,6 and Ant2,7 underwent self-aggregation to a remarkable extent as shown by spectroscopic analysis (see Supplementary Material, Fig S2) and, notably, they effectively induced double-stranded DNA (dsDNA) precipitation even at the lowest binding ratios examined. Therefore, a quantitative evaluation of their interaction with dsDNA was not performed, but it can be safely stated that the drugs interact efficiently with the double helix.

The aforementioned results indicate Ant1,5 as the most promising G-quadruplex binder of the series. Fluorometric titrations were performed to quantify the binding process of Ant1,5 to the folded telomeric sequence using Ant9,10 for comparison. Both compounds are fluorescent and their quantum yield is enhanced upon binding to the G-quadruplex. The binding isotherms, determined at 0.5 M ionic strength to avoid unspecific electrostatic interactions, confirmed a remarkable difference in quadruplex DNA recognition by the two derivatives (Fig. 4). As suggested by Job plot analysis, we used a 1:1 binding model to examine experimental data. The results, summarized in Table 1, showed a remarkably stronger (one order of magnitude) complexation by Ant1,5 than by Ant9,10. As regard dsDNA, both derivatives showed comparable binding constants, again one order of magnitude lower than the constant exhibited by Ant1,5 for quadruplex DNA.

Table 1
Thermodynamic binding parameter for the interaction of tested derivatives with different DNA foldings.

Compound	Tel22		Calf thymus DNA	
	$Ka \times 10^{-6}$ (M^{-1})	n[a]	$Ka \times 10^{-6}$ (M^{-1})	n[b]
Ant1,5	4.12 ± 0.25	1	0.32 ± 0.02	3.4
Ant9,10	0.46 ± 0.02	1	0.29 ± 0.02	4.9

[a] For Tel22, n refers to G-quadruplex involved in drug binding.
[b] For calf thymus DNA, *n* refers to residue involved in drug binding.

Table 2
IC_{50} values (μM) determined for *Taq* polymerase and telomerase for all tested compounds.

Compound	*Taq* polymerase	Telomerase
Ant1	>40	–
Ant1,5	30.0 ± 5.0	0.9 ± 0.2
Ant1,8	30.0 ± 5.0	7.5 ± 2.0
Ant2	>40	–
Ant2,6	30.0 ± 5.0	1.9 ± 0.5
Ant2,7	7.5 ± 2.0	1.9 ± 0.5
Ant9	>40	–
Ant9,10 (Bis)	15.0 ± 3.0	3.8 ± 1.0

3.3. Telomerase inhibition correlates with G-quadruplex recognition

The effects of bisantrene analogues on telomerase activity were evaluated by TRAP assay using cellular extracts of the JR8 human melanoma cell line in the presence of different concentration of the drugs (0–40 μM). In parallel, all compounds were additionally analyzed for their *Taq* polymerase inhibition properties.

The results obtained from enzymatic assays are summarized in Table 2, where IC_{50} values for telomerase and *Taq* polymerase are reported. According to their poor DNA affinity, mono-substituted anthracene derivatives Ant1, Ant2 and Ant9 showed no inhibitory properties towards the two enzymes. All bis-substituted derivatives were able to efficiently interfere with tested enzymes: Ant9,10 and Ant2,7 proved to be the most active in inhibiting *Taq* polymerase activity. In turn, Ant1,5, Ant2,6 and Ant2,7 were the most efficient against telomerase, with IC_{50} values in the low micromolar range (IC_{50} 0.9, 1.9 and 1.9 μM, respectively).

To rule out possible artifacts due to the presence of the ligand during the PCR step in the telomerase inhibitory assay, Ant1,5 (the most active telomerase inhibitor) was added after the telomerase extension step. In this case, we observed a concentration-dependent reduction in product amplification that allowed us to estimate an IC_{50} value at about 3.7 μM for Ant1,5-mediated inhibition of *Taq* polymerase amplification of these G-rich DNA fragments. Therefore, although Ant1,5 can affect the PCR step, a range of concentrations is available to selectively inhibit telomerase without affecting *Taq* polymerase activity.

In turn, similar experiments performed with the other bis-substituted derivatives showed no window for specific telomerase inhibition.

On the basis of the above results, Ant1,5 appeared worthy of further examination.

3.4. Ant1,5 induces antiproliferative effects and a DNA damage response at the telomeric level in telomerase-positive and ALT-positive tumor cells

The results so far presented were obtained in a cell-free system, which might not fully reflect the intracellular environment. To

Table 3
IC_{50} values (μM) obtained in SK-Mel5 and LoVo cell lines exposed to the indicated bisantrene analogues.

Compound	IC_{50} (μM)			
	SK-Mel5		LoVo	
	24 h	96 h	24 h	96 h
Ant9	5.4 ± 1.5	4.9 ± 1.2	4.0 ± 1.0	1.5 ± 0.8
Ant9,10	1.5 ± 0.8	1.4 ± 0.8	4.8 ± 1.0	1.4 ± 0.8
Ant1,5	12.6 ± 3.0	13.0 ± 4.0	>20	>20
Ant1,8	3.7 ± 1.0	6.8 ± 2.0	10.8 ± 3.0	6.4 ± 2.0
Ant2,6	1.8 ± 0.9	1.4 ± 0.8	2.2 ± 0.9	1.3 ± 0.8
Ant2,7	9.0 ± 3.0	7.4 ± 2.0	14.3 ± 4.0	5.9 ± 2.0

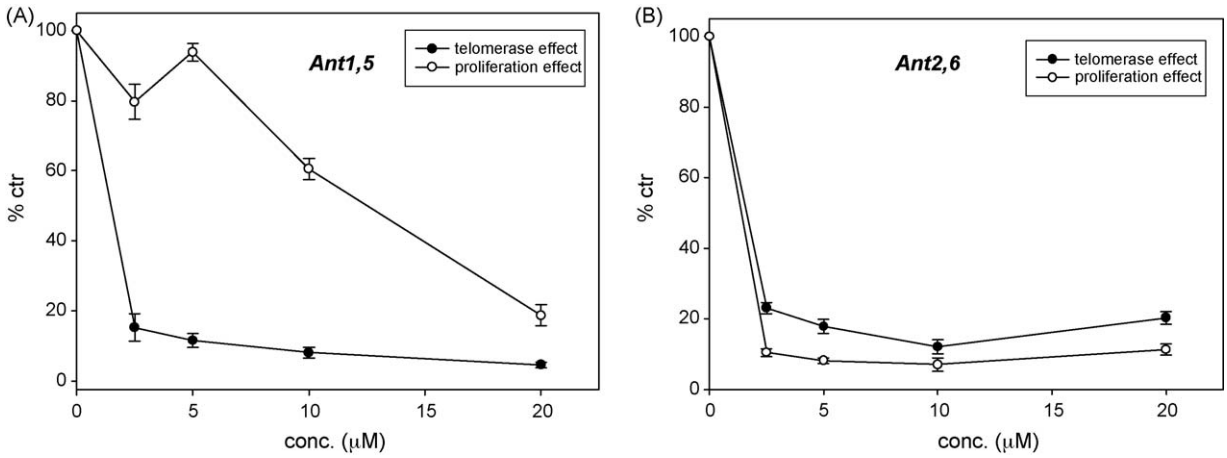

Fig. 5. Effect of Ant1,5 (a) and Ant2,6 (b) on the proliferative potential (○) and telomerase activity (●) of SK-Mel5 cells after 24 h of drug treatment. Data are reported as percentage with respect to untreated cells and represent mean values ± SD of three independent experiments.

evaluate the biological effects induced by mono- and bis-substituted bisantrene analogues, human melanoma (SK-Mel5) and colon cancer (LoVo) cell lines, both constitutively expressing telomerase activity as determined by TRAP assay (data not shown), were used. Cells were exposed to different concentrations of tested derivatives ranging from 2.5 to 20 μM for 24 and 96 h at 37 °C. IC_{50} values summarized in Table 3 suggest that Ant1,5 is the least cytotoxic compound among those tested on both cell lines, showing IC_{50} values of 13 μM in SK-Mel5 and >20 μM in LoVo cells after 96 h of drug exposure.

To better understand the relevance of telomerase inhibition for the cell growth impairment induced by tested compounds, we analyzed telomerase activity in protein extracts after a 24-h exposure to different drug concentrations and compared it with the cell proliferation data. Interestingly, inhibition of telomerase activity on treated SK-Mel5 cells occurred at a lower Ant1,5 concentration than did cell growth reduction, thus producing a good selectivity window between antitelomerase activity and antiproliferative effects (Fig. 5a). Such behavior was not observed with any of the other derivatives (mono- and bi-substituted ones) where telomerase inhibition paralleled drug-induced cytotoxicity, as exemplified for Ant2,6 in Fig. 5b.

To assess delayed antiproliferative effects, we prolonged cell treatment with Ant1,5 for up to 8 days. Cells were exposed to a

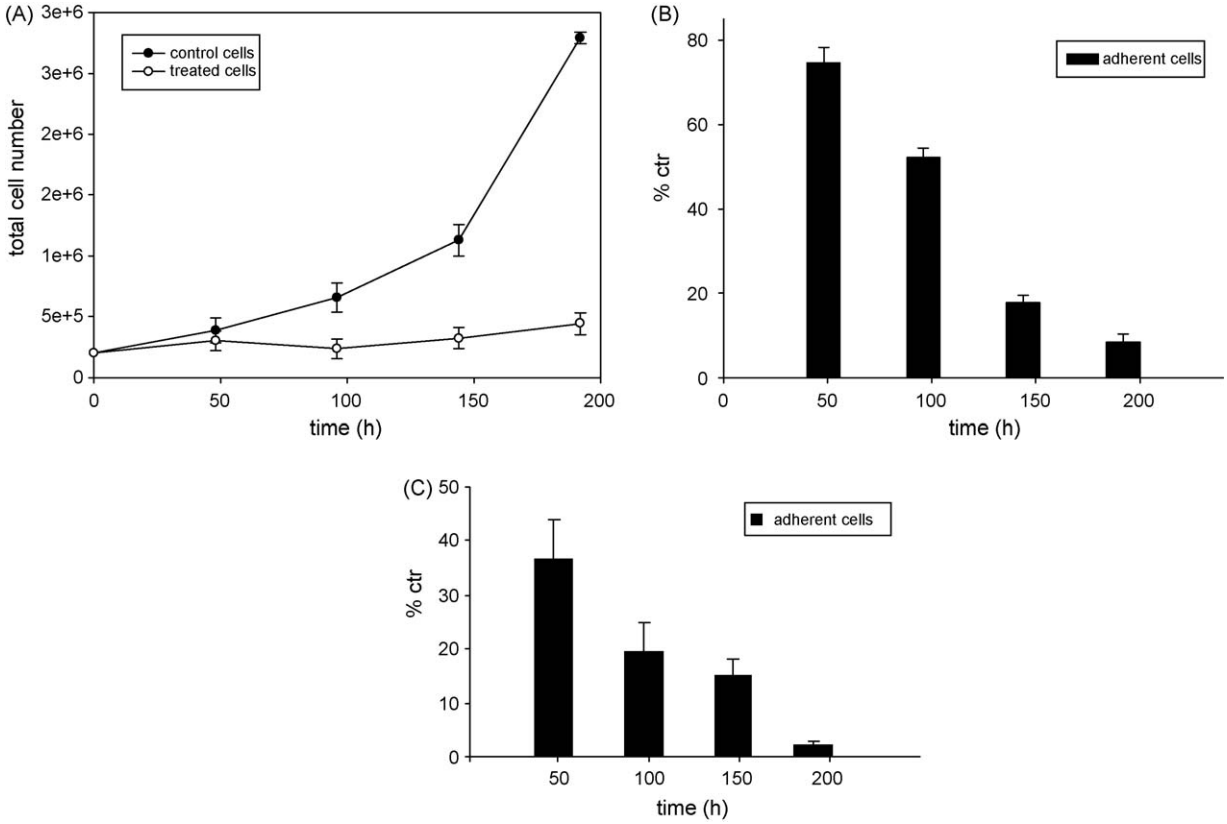

Fig. 6. (a) Cell growth curves of untreated (●) or Ant1,5-treated SK-Mel5 (○) cells. Data are expressed as total cell number (i.e., adherent + floating cells) and represent mean values ± SD of three independent experiments. The time-dependent reduction in the number of adherent SK-Mel5 (b) and U2OS cells (c) exposed to Ant1,5 is also shown. Data are reported as percentage of growing cells, with respect to untreated cells, and represent mean values ± SD of three independent experiments.

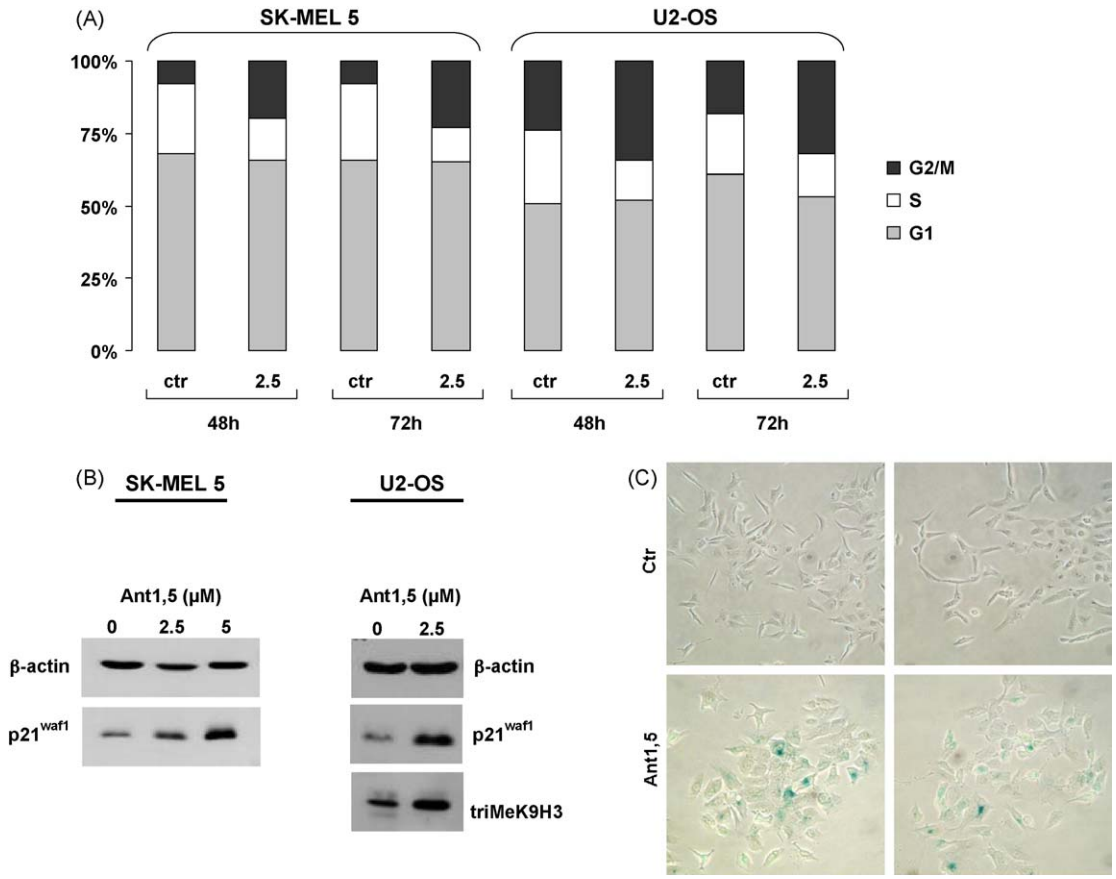

Fig. 7. (a) Percentage of SK-Mel5 and U2OS cells throughout the different phases of the cell cycle, as assessed by flow cytometry in untreated (ctr) or Ant1,5-treated cells (2.5 μM). (b) Representative western blotting showing the effect of a 48-h exposure to Ant1,5 on the expression of $p21^{waf1}$ and trymethyl K9 histone H3 (triMeK9H3) in SK-Mel5 and U2OS cells. Anti-β-actin monoclonal antibody was used to ensure equal loading of proteins. (c) Representative photomicrographs showing the induction of cellular senescence in Ant1,5-treated U2OS cells compared to control, as assessed by senescence-associated β-galactosidase staining. Magnification: ×40.

fixed concentration of compound (2.5 μM), which grants a good selectivity window between telomerase inhibition and cell growth impairment (Fig. 5a). Drug treatment was repeated every 48 h, and cell number was assessed every 2 days. As reported in Fig. 6a, control cells showed an exponential growth during the time course of the experiment. Instead, the total number of Ant1,5-treated cells remained essentially constant at the different time points, although a more detailed analysis revealed a progressive reduction in the number of adherent cells associated to an increase in floating cell number (Fig. 6b). Interestingly, fluorescence microscopy analysis after cell staining with propidium iodide did not evidence apoptosis in floating SK-Mel5 cells at the different time points considered (data not shown).

The ability of Ant1,5 to impair the proliferative potential of telomerase-negative tumor cells, known to maintain their telomeres by the ALT mechanism, was also investigated. Specifically, the ALT-positive U2OS human osteogenic sarcoma cell line was exposed to 2.5 μM Ant1,5 for 48 h, and the effect on cell growth was determined at different intervals from the beginning of treatment. A time-dependent reduction in the number of drug-treated cells with respect to control was observed, with an almost complete abrogation of cell proliferation at day 8 (Fig. 6c). Again, no evidence of apoptotic cells was found by fluorescence microscopy (data not shown). Flow cytometric analysis confirmed the absence of apoptosis since no pre-G1 apoptotic peak was detected in Ant1,5-treated U2OS cultures at different intervals from drug exposure. However, an increased accumulation of cells in the G2/M compartment with a concomitant reduction in the S-phase cell fraction was consistently observed in drug-treated cells (Fig. 7a). A similar drug-induced cell cycle impairment was observed in telomerase-positive SK-Mel5 cells (Fig. 7a).

To test the hypothesis that Ant1,5-caused growth arrest could be due to the induction of senescence, we analyzed the expression of the cyclin-dependent kinase inhibitor $p21^{waf1}$, which is known to be involved in a senescence pathway triggered by telomere dysfunction [33]. We found that $p21^{waf1}$protein expression was markedly enhanced in both SK-Mel5 and U2OS cell lines following drug exposure (Fig. 7b). In addition, an increased expression of trimethyl K9 histone H3 – a marker suggestive of cellular senescence-associated changes in chromatin structure [34] – was observed in Ant1,5-treated U2OS cells (Fig. 7b). The induction of cellular senescence was also confirmed by staining for senescence-associated β-galactosidase. Specifically, results showed that either SK-Mel5 or U2OS cells exposed to Ant1,5 were characterized by a marked increase in β-galactosidase activity compared to untreated cells (Fig. 7c and data not shown). Furthermore, in drug-treated cells, the induction of DNA damage, as gauged by the nuclear accumulation of γH2AX, was also observed. Specifically, a significant increase in the percentage of cells harboring DNA damage (>5 γH2AX foci/nucleus) was appreciable in SK-Mel 5 and U2OS cultures exposed to Ant1,5 (Fig. 8a). To test whether the DNA damage foci was due, at least in part, to drug-induced telomere dysfunction, the localization of γH2AX foci at the telomere was determined by combined γH2AX immunofluorescence and telomere fluorescence *in situ* hybridization in U2OS cells. Results showed the co-localization of the signals, indicating the induction of a DNA damage response at the telomere level (Fig. 8b).

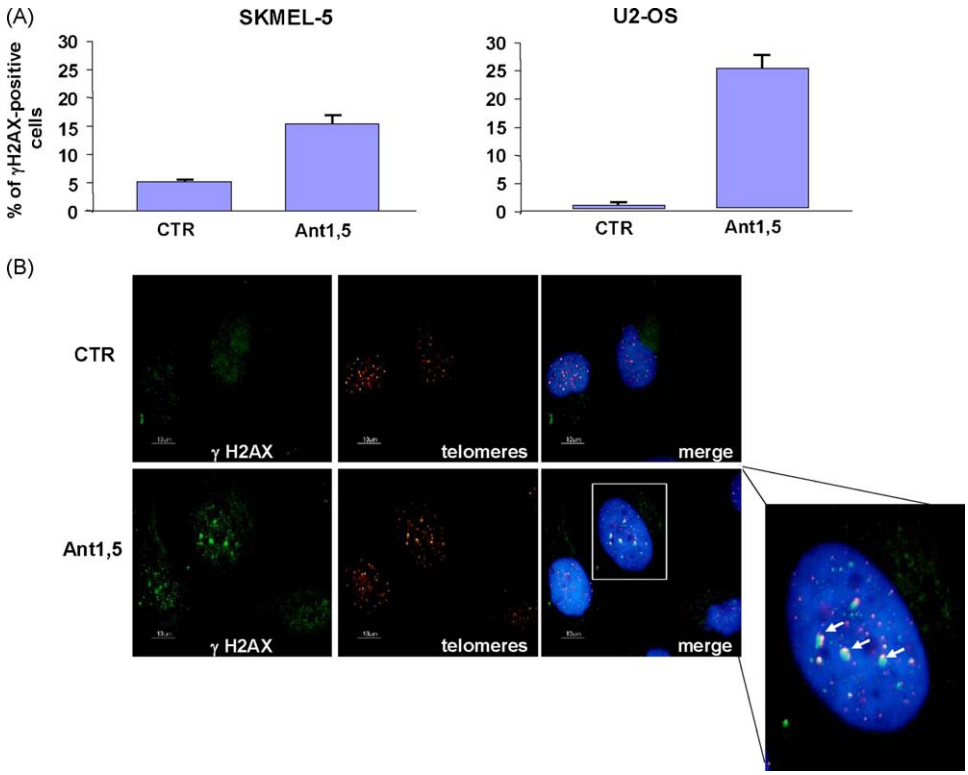

Fig. 8. (a) Quantification of γH2AX foci in untreated or Ant1,5-treated SK-Mel5 and U2OS cells. Data are reported as percentage of γH2AX-positive cells in the overall cell population (mean values ± SD of three independent determinations). (b) Representative images of combined γH2AX immunofluorescence and telomere fluorescence *in situ* hybridization in untreated (ctr) or Ant1,5-treated U2OS cells.

4. Discussion

The efficient and selective recognition of G-quadruplex structures by rationally designed small ligands is still an open issue. The novel compounds reported here were designed based on previous structure–activity relationship studies concerning bis-substituted planar tricyclic chromophores, mainly amido-anthraquinones [13,14,24,35–39] and acridines [24,40–42]. They indicated that at least two side chains with amine groups protonable at physiological pH are required for G-quadruplex binding. Here, we explored the yet unknown effects of the pattern of substitution on an anthracene scaffold. The 4,5-dihydro-1H-imidazol-2-yl hydrazone side chain was chosen because it is found in bisantrene (Ant9,10), one of the most efficient anthracene-based dsDNA binders thus far known [24]. Bisantrene is believed to intercalate between adjacent base pairs of double-stranded DNA through π–π stacking, with side chains located in either groove (threading mode), which grants affinity constants well above $10^6\ M^{-1}$ at physiological conditions [43].

As regard the number of side chains, using double-stranded DNA we previously confirmed that, irrespectively of their position, the presence of at least two protonable side chains remarkably improves DNA affinity. The same holds true for G-quadruplex binding. This is not unexpected since G-quadruplex exhibits an even higher negative charge density than dsDNA. Interestingly, for bisantrene congeners, the requirement for at least two side chains is not simply related to an increase in total charge of the ligand to promote more effective ionic interactions with the nucleic acid. Indeed, different regioisomers showed distinct binding affinities for telomeric G-quadruplex, the ranking order being Ant1,5 ≥ Ant2,7 ≈ Ant2,6 > Ant9,10 ≈ Ant1,8. Interestingly, G-quadruplex binding is well related to induction of the folded structure by our Ant derivatives, which confirms their ability to shift nucleic acid conformational equilibrium upon binding. The fact that the most efficient G-quadruplex binders are substituted on two distinct aromatic rings with side chains pointing in opposite directions with reference to the long axis of the aromatic system likely suggests formation of additional specific interactions between the 4,5-dihydro-1H-imidazol-2-yl hydrazone groups and the G-quadruplex structure.

Such behavior is distinct from that observed with 1,4; 1,5; 1,8; 2,6 and 2,7 anthraquinone regioisomer, for which the side chains' position does not drastically alter the G-quadruplex affinity but influences the binding mode [44]. Indeed, the aromatic surface can slide over the G-quartet to optimally conjugate stacking and side chains ionic interactions in the grooves, thus resulting in comparable binding affinity for all tested regioisomers [13]. In turn, the behavior of bisantrene analogues is somehow reminiscent of bis-substituted acridine derivatives, where the protonated N11 lies in the G-quartet plane, which possibly reduces the number of available acridine geometries for efficient stacking and, consequently, produces a differential affinity for different regioisomers [40,45].

Two main differences distinguish our derivatives from acridines or anthracenediones: the first is the aromatic system, which in our case is not characterized by the presence of a localized charge density on the aromatic system. This should grant high flexibility of location over the G-quartet. The second difference lies in the nature of the side chains. They can easily rotate around the C–C bond connecting them to the anthracene ring system [26]. However, they are more rigid and planar, besides being chemically distinct, than those introduced on AQ or AC (generally optimal activity requires a $-(CH_2)_2-$ linker and a piperidine/piperazine terminal group) [44]. Thus, their peculiar skeleton likely locks the aromatic tricyclic portion to a defined position onto the G-quartet to maximize favorable interactions.

Another interesting biophysical result, peculiar of the bisantrene structural type, is the selectivity (difference in affinity by one order of magnitude) exhibited by Ant1,5 for G-quadruplex versus double-stranded DNA binding. In fact, bis-substituted anthraquinone and acridine congeners are not able to discriminate between the above DNA arrangements and notable improvement in terms of G-quadruplex affinity. Selectivity can be obtained only by incrementing the number of side chains (three in BRACO19) [17,18].

The biological relevance of G-quadruplex binding by tested derivatives is evidenced by the good correlation found between telomerase inhibition and G-quadruplex stabilization or induction, clearly supporting an involvement of G-quadruplex interaction in drug-mediated telomerase inhibition. It is noteworthy that G-quadruplex binding, stabilization and induction are well related, suggesting their possible relevance at the cellular level, where the target telomeric nucleic acid can assume different conformations. Actually, the biophysical results are in line with the cellular data, with Ant1,5 exhibiting the most favorable balance between G-quadruplex and dsDNA recognition and showing a significant gap and between telomerase inhibition cell cytoxicity. On the contrary, the high cytotoxicity level of the other regioisomers suggests the prevalence of other non telomerase-mediated mechanisms of cell death. In particular, for the G-quadruplex binders Ant2,6 and Ant2,7, elevated toxicity is in line with their high affinity for dsDNA.

Another relevant point we experimentally confirmed is the ability of Ant1,5 to act both at the telomerase level, by interfering with substrate recognition (hence suppressing its catalytic activity), and at the telomere level, by modifying its structural organization. In fact, we found that Ant1,5 affects telomere function not only in telomerase-expressing cells but also in ALT-positive cell lines, since it consistently provokes a DNA damage response, as evidenced by the formation of γH2AX foci that partially co-localize at the telomere, in agreement with results reported for telomestatin [46]. For Ant1,5, such a DNA damage response, together with the absence of apoptosis and the induction of cell cycle impairment (mainly G2M phase arrest), suggest a drug-mediated activation of a senescence pathway [47]. Such behavior can help explain the cell proliferation inhibition observed in ALT cell lines treated with other G-quadruplex binders structurally distinct from ours, such as pentacyclic acridines [48], triazine derivatives [19] and fluoroquinoanthroxazines [49]. The common cell growth impairment we observed in telomerase- and ALT-positive cell lines suggests that telomerase apparently does not represent the anthracene primary target, the concomitant key event likely consisting in an alteration of telomere architecture, which is sensed by the cell as a DNA damage event. In both pathways, the driving force is likely G-quadruplex recognition, as supported by the modulation of cellular effects according to the regioisomeric substitution pattern.

Overall, results obtained with Ant1,5 highlight the opportunity to clinically develop agents which impair cell growth through direct interference with telomeres, that could also be exploited for the treatment of tumors expressing telomere maintenance mechanisms alternative to telomerase.

Acknowledgment

This work was funded by Associazione Italiana per la Ricerca sul Cancro.

Appendix A. Supplementary data

Supplementary data associated with this article can be found, in the online version, at doi:10.1016/j.bcp.2010.02.018.

References

[1] Greider CW, Blackburn EH. Identification of a specific telomere terminal transferase activity in Tetrahymena extracts. Cell 1985;43:405–13.
[2] Shay JW, Bacchetti S. A survey of telomerase activity in human cancer. Eur J Cancer 1997;33:787–91.
[3] Folini M, Gandellini P, Zaffaroni N. Targeting the telosome: therapeutic implications. Biochim Biophys Acta 2009;1792:309–16.
[4] Hahn WC, Stewart SA, Brooks MW, York SG, Eaton E, Kurachi A, et al. Inhibition of telomerase limits the growth of human cancer cells. Nat Med 1999;5:1164–70.
[5] de Lange T. Shelterin: the protein complex that shapes and safeguards human telomeres. Genes Dev 2005;19:2100–10.
[6] Deng Y, Chan SS, Chang S. Telomere dysfunction and tumour suppression: the senescence connection. Nat Rev Cancer 2008;8:450–8.
[7] Neidle S. The structures of quadruplex nucleic acids and their drug complexes. Curr Opin Struct Biol 2009;19:239–50.
[8] De Cian A, Lacroix L, Douarre C, Temime-Smaali N, Trentesaux C, Riou JF, et al. Targeting telomeres and telomerase. Biochimie 2008;90:131–55.
[9] Huppert JL. Four-stranded nucleic acids: structure, function and targeting of G-quadruplexes. Chem Soc Rev 2008;37:1375–84.
[10] Davis J. AngewantdteChemie 2004;43:668–98.
[11] Zahler AM, Williamson JR, Cech TR, Prescott DM. Inhibition of telomerase by G-quartet DNA structures. Nature 1991;350:718–20.
[12] Salvati E, Leonetti C, Rizzo A, Scarsella M, Mottolese M, Galati R, et al. Telomere damage induced by the G-quadruplex ligand RHPS4 has an antitumor effect. J Clin Invest 2007;117:3236–47.
[13] Perry PJ, Reszka AP, Wood AA, Read MA, Gowan SM, Dosanjh HS, et al. Human telomerase inhibition by regioisomeric disubstituted amidoanthracene-9,10-diones. J Med Chem 1998;41:4873–84.
[14] Huang HS, Chen IB, Huang KF, Lu WC, Shieh FY, Huang YY, et al. Synthesis and human telomerase inhibition of a series of regioisomeric disubstituted amidoanthraquinones. Chem Pharm Bull (Tokyo) 2007;55:284–92.
[15] Sun D, Thompson B, Cathers BE, Salazar M, Kerwin SM, Trent JO, et al. Inhibition of human telomerase by a G-quadruplex-interactive compound. J Med Chem 1997;40:2113–6.
[16] Perry PJ, Read MA, Davies RT, Gowan SM, Reszka AP, Wood AA, et al. 2,7-Disubstituted amidofluorenone derivatives as inhibitors of human telomerase. J Med Chem 1999;42:2679–84.
[17] Read M, Harrison RJ, Romagnoli B, Tanious FA, Gowan SH, Reszka AP, et al. Structure-based design of selective and potent G quadruplex-mediated telomerase inhibitors. Proc Natl Acad Sci USA 2001;98:4844–9.
[18] Harrison RJ, Cuesta J, Chessari G, Read MA, Basra SK, Reszka AP, et al. Trisubstituted acridine derivatives as potent and selective telomerase inhibitors. J Med Chem 2003;46:4463–76.
[19] Riou JF, Guittat L, Mailliet P, Laoui A, Renou E, Petitgenet O, et al. Cell senescence and telomere shortening induced by a new series of specific G-quadruplex DNA ligands. Proc Natl Acad Sci USA 2002;99:2672–7.
[20] Izbicka E, Wheelhouse RT, Raymond E, Davidson KK, Lawrence RA, Sun D, et al. Effects of cationic porphyrins as G-quadruplex interactive agents in human tumor cells. Cancer Res 1999;59:639–44.
[21] Han H, Cliff CL, Hurley LH. Accelerated assembly of G-quadruplex structures by a small molecule. Biochemistry 1999;38:6981–6.
[22] Dai J, Punchihewa C, Ambrus A, Chen D, Jones RA, Yang D. Structure of the intramolecular human telomeric G-quadruplex in potassium solution: a novel adenine triple formation. Nucleic Acids Res 2007;35:2440–50.
[23] Venitt S, Crofton-Sleigh C, Agbandje M, Jenkins TC, Neidle S. Anthracene-9,10-diones as potential anticancer agents: bacterial mutation studies of amido-substituted derivatives reveal an unexpected lack of mutagenicity. J Med Chem 1998;41:3748–52.
[24] Read MA, Wood AA, Harrison JR, Gowan SM, Kelland LR, Dosanjh HS, et al. Molecular modeling studies on G-quadruplex complexes of telomerase inhibitors: structure-activity relationships. J Med Chem 1999;42:4538–46.
[25] Elliott JA, Wilson WD, Shea RG, Hartley JA, Reszka K, Lown JW. Interaction of bisantrene anti-cancer agents with DNA: footprinting, structural requirements for DNA unwinding, kinetics and mechanism of binding and correlation of structural and kinetic parameters with anti-cancer activity. Anticancer Drug Des 1989;3:271–82.
[26] Capranico G, Guano F, Moro S, Zagotto G, Sissi C, Gatto B, et al. Mapping drug interactions at the covalent topoisomerase II-DNA complex by bisantrene/amsacrine congeners. J Biol Chem 1998;273:12732–9.
[27] Sissi C, Bolgan L, Moro S, Zagotto G, Bailly C, Menta E, et al. DNA-binding preferences of bisantrene analogues: relevance to the sequence specificity of drug-mediated topoisomerase II poisoning. Mol Pharmacol 1998;54:1036–45.
[28] Zagotto G, Oliva A, Guano F, Menta E, Capranico G, Palumbo M. Synthesis, DNA-damaging and cytotoxic properties of novel topoisomerase II-directed bisantrene analogues. Bioorg Med Chem Lett 1998;8:121–6.
[29] Neumann AA, Reddel RR. Telomere maintenance and cancer—look, no telomerase. Nat Rev Cancer 2002;2:879–84.
[30] Costa A, Daidone MG, Daprai L, Villa R, Cantu S, Pilotti S, et al. Telomere maintenance mechanisms in liposarcomas: association with histologic subtypes and disease progression. Cancer Res 2006;66:8918–24.
[31] McGhee JD, von Hippel PH. Theoretical aspects of DNA-protein interactions: co-operative and non-co-operative binding of large ligands to a one-dimensional homogeneous lattice. J Mol Biol 1974;86:469–89.

[32] Ambrus A, Chen D, Dai J, Bialis T, Jones RA, Yang D. Human telomeric sequence forms a hybrid-type intramolecular G-quadruplex structure with mixed parallel/antiparallel strands in potassium solution. Nucleic Acids Res 2006;34:2723–35.
[33] Herbig U, Sedivy JM. Regulation of growth arrest in senescence: telomere damage is not the end of the story. Mech Ageing Dev 2006;127:16–24.
[34] Wu CH, van Riggelen J, Yetil A, Fan AC, Bachireddy P, Felsher DW. Cellular senescence is an important mechanism of tumor regression upon c-Myc inactivation. Proc Natl Acad Sci USA 2007;104:13028–33.
[35] Perry PJ, Gowan SM, Reszka AP, Polucci P, Jenkins TC, Kelland LR, et al. 1,4- and 2,6-disubstituted amidoanthracene-9,10-dione derivatives as inhibitors of human telomerase. J Med Chem 1998;41:3253–60.
[36] Huang HS, Chiou JF, Fong Y, Hou CC, Lu YC, Wang JY, et al. Activation of human telomerase reverse transcriptase expression by some new symmetrical bis-substituted derivatives of the anthraquinone. J Med Chem 2003;46:3300–7.
[37] Huang HS, Huang KF, Li CL, Huang YY, Chiang YH, Huang FC, et al. Synthesis, human telomerase inhibition and anti-proliferative studies of a series of 2,7-bis-substituted amido-anthraquinone derivatives. Bioorg Med Chem 2008;16:6976–86.
[38] Huang HS, Chou CL, Guo CL, Yuan CL, Lu YC, Shieh FY, et al. Human telomerase inhibition and cytotoxicity of regioisomeric disubstituted amidoanthraquinones and aminoanthraquinones. Bioorg Med Chem 2005;13:1435–44.
[39] Cairns D, Michalitsi E, Jenkins TC, Mackay SP. Molecular modelling and cytotoxicity of substituted anthraquinones as inhibitors of human telomerase. Bioorg Med Chem 2002;10:803–7.
[40] Harrison RJ, Reszka AP, Haider SM, Romagnoli B, Morrell J, Read MA, et al. Evaluation of by disubstituted acridone derivatives as telomerase inhibitors: the importance of G-quadruplex binding. Bioorg Med Chem Lett 2004;14:5845–9.
[41] Laronze-Cochard M, Kim YM, Brassart B, Riou JF, Laronze JY, Sapi J. Synthesis and biological evaluation of novel 4,5-bis(dialkylaminoalkyl)-substituted acridines as potent telomeric G-quadruplex ligands. Eur J Med Chem 2009;44:3880–8.
[42] Harrison RJ, Gowan SM, Kelland LR, Neidle S. Human telomerase inhibition by substituted acridine derivatives. Bioorg Med Chem Lett 1999;9:2463–8.
[43] Yao S, Wilson WD. 1D and 2D 1H NMR studies on bisantrene complexes with short DNA oligomers. Sci China B 1995;38:1462–72.
[44] Neidle S, Read MA. G-quadruplexes as therapeutic targets. Biopolymers 2000;56:195–208.
[45] Campbell NH, Parkinson GN, Reszka AP, Neidle S. Structural basis of DNA quadruplex recognition by an acridine drug. J Am Chem Soc 2008;130:6722–4.
[46] Temime-Smaali N, Guittat L, Sidibe A, Shin-ya K, Trentesaux C, Riou JF. The G-quadruplex ligand telomestatin impairs binding of topoisomerase IIIalpha to G-quadruplex-forming oligonucleotides and uncaps telomeres in ALT cells. PLoS One 2009;4:e6919.
[47] von Zglinicki T, Saretzki G, Ladhoff J, d'Adda di Fagagna F, Jackson SP. Human cell senescence as a DNA damage response. Mech Age Dev 2005;126:111–7.
[48] Gowan SM, Heald R, Stevens MF, Kelland LR. Potent inhibition of telomerase by small-molecule pentacyclic acridines capable of interacting with G-quadruplexes. Mol Pharmacol 2001;60:981–8.
[49] Kim MY, Duan W, Gleason-Guzman M, Hurley LH. Design, synthesis, and biological evaluation of a series of fluoroquinoanthroxazines with contrasting dual mechanisms of action against topoisomerase II and G-quadruplexes. J Med Chem 2003;46:571–83.